PROCEEDINGS, 41st Workshop on Geothermal Reservoir Engineering
Stanford University, Stanford, California, February 22-24, 2016
SGP-TR-209

3D VSP Experiment Design Study of the Raft River Geothermal Field

Gregory A. Newman and Peter V. Petrov

Lawrence Berkeley National Laboratory, One Cyclotron Road, Berkeley CA, 94720 USA

Corresponding author: gnewman@lbl.gov

Keywords: Vertical Seismic Profiling; 3D Full Waveform Inversion; Raft River

ABSTRACT

Geothermal systems are, in many cases, characterized by complex geological structures with discernible anomalous zones, related to the presence of geothermal fluids. Development of geothermal energy production increasing requires more accurate information on fault distributions, and paths of or barriers to fluid flow within the reservoir. Toward this purpose, we have embarked upon a survey design study using vertical seismic profiling (VSP) measurements for imaging seismic attributes within the Narrows Zone, a striking geological feature, which strongly controls permeability and fluid flow within the Raft River geothermal reservoir. The geothermal field is located in Cassia County in southwestern Idaho and is the site of a Department of Energy Enhanced Geothermal System (EGS) project. Motivating this study is our plans to acquire VSP data later this this year at Raft River. Full waveform inversion (FWI) of simulated data with frequency content between 5 through 15 Hz has been analyzed and is presented. The data arise from a 3D elastic model of the Narrows Zone, developed by Hi-Q and the University of Utah. Our goal is to determine acceptable survey design parameters needed for 3D imaging of elastic attributes within anticipated survey cost.

1. INTRODUCTION

The Raft River geothermal area (Fig.1a) is within the northern part of the Basin and Range, near the southern periphery of the Snake River plain. It is located in Raft River valley, a north-south trending Cenozoic basin (Williams et al. 1982), east of the Albion and Jim Sage mountains, west of the Black Pine mountains, and north of the Raft River range. Mid-Tertiary metamorphic core complexes are associated with the Albion and Raft River mountains. The valley is filled with approximately 2 km of Pleistocene Raft River Formation alluvium and Mid-Tertiary Salt Lake Formation sediments, conglomerate and volcanic rocks, which overly gently, east-dipping Precambrian basement of quartzite, schist and quartz monzonite. The basement contact is inferred to be a detachment surface, into which the Bridge and Horse Wells listric fault zones are believed to sole. The Narrows Zone (Fig.1b)), a northeast-southwest trending basement shear zone is very important feature in controlling the reservoir structural boundaries. It has been inferred from geophysical data (Mabey et al., 1978), where production is generally from the Precambrian basement, at ~ 140 C from depths of 1400 to 1750 m (Ayling et al., 2011; Jones et al., 2011). Geochemical analysis by Ayling et al. (2011) finds distinct geothermal fluid geochemistries in the southeast (SE) and northwest (NW) parts of the field.

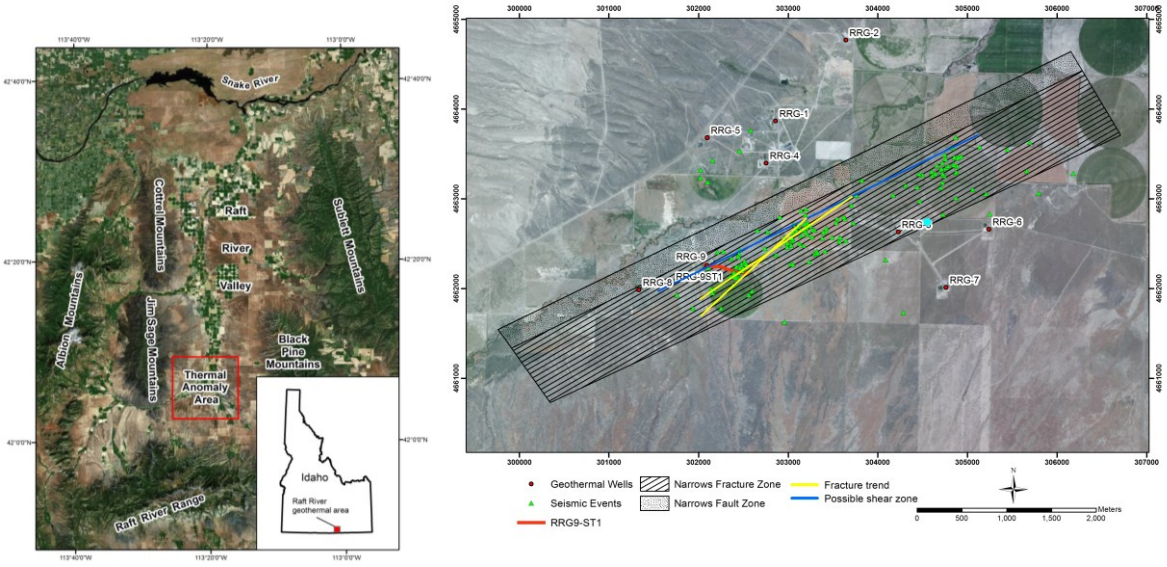

Figure 1: (a) Raft River Geothermal Area. (b) Well Locations Relative to Narrows Zone (hashed structure).

Because the importance of the Narrows Zone on production and distribution of geothermal fluids at Raft River, more accurate information on fault distributions, and paths of or barriers to fluid flow within this zone is necessary for enhanced geothermal systems (EGS) development. Active seismic data acquired from 3D vertical seismic profiling (VSP) has the potential to provide new and significant information for mapping fracture permeability in EGS reservoirs that has not been previously attainable. In a pilot project to demonstrate such potential, VSP data later this this year will be acquired at the Raft River well RG9 (Figure 1b), which penetrates the Narrows Zone In this paper we report on a survey design study on VSP acquisition for imaging seismic attributes within the Narrows Zone. The study employs a 3D elastic full waveform imaging (FWI) method on simulated data in the Laplace-Fourier domain, with frequency content between 5 through 15 Hz.

2. ELASTIC FWI METHOD

Three-dimensional full-waveform inversion (FWI) is an advanced seismic imaging technique that has recently become more computationally feasible and more frequently employed within the oil and gas industry (Kapoor et al., 2013, Plessix *et al.* 2010 and Sirgue *et al.* 2010). It is well known that FWI can be used to successfully update subsurface seismic attributes at relevant exploration depths, provided the acquired data contain sufficient number of frequencies and offsets. However, for computational reasons, most 3D applications still employ acoustic modeling assumptions, thereby neglecting elastic effects (Plessix *et al.* 2010, Sirgue *et al.* 2010).

Elastic FWI applications are mainly performed in 2D (e.g., Brossier et al. 2009 and 2015, Köhn *et al.* 2012). Unfortunately, the 2D approximation is unable to describe scattering effects arising from 3D heterogeneous subsurface structures and is incompatible with typical 3D data acquisition geometries employed in practice.

2.1 3D Laplace-Fourier Domain FWI

Generally, the elastic FWI problem in Laplace Fourier domain is defined as determining an elastic attribute model $\mathbf{m} = (b, \kappa, \mu)$ (bulk and shear moduli κ, μ and buoyancy $b = 1/\rho$, where ρ is mass density), which minimizes an objective functional expressed by the residuals between the model responses and the observed data $\phi_d(\mathbf{m})$ for complex frequency *s*. To stabilize the inversion process a model smoothness constraint $\phi_m(\mathbf{m})$ for complex frequency is added to $\phi_d(\mathbf{m})$. Specifically we write

$$\begin{aligned} \phi(\mathbf{m}) &= \phi_d(\mathbf{m}) + \phi_m(\mathbf{m}), \\ \phi_d(\mathbf{m}) &= \sum_{q,s_k} \left(\mathbf{d}_q^{obs}(s_k) - \mathbf{d}_q^{sim}(\mathbf{m}, s_k)\right)^H \mathbf{E}^H \mathbf{E} \left(\mathbf{d}_q^{obs}(s_k) - \mathbf{d}_q^{sim}(\mathbf{m}, s_k)\right), \\ \phi_m(\mathbf{m}) &= \lambda \mathbf{m}^T \mathbf{W}^T \mathbf{W}\, \mathbf{m}. \end{aligned} \tag{1}$$

In eq. (1) $\mathbf{d}_q^{obs}(s_k), \mathbf{d}_q^{sim}(\mathbf{m}, s_k)$ are the observed and predicted data vectors, with subscript q indicating the source position, $\mathbf{E}$ is the diagonal matrix of weights defined by the data error, $\mathbf{W}$ is the regularization matrix, which consists of a finite-difference approximation to the gradient operator (∇_m), λ is the regularization parameter to balance data error and the model smoothness constraint, and symbols "H, T" denote the Hermitian conjugate and transpose operations, respectively. The observed data vectors consist of the Laplace-Fourier image of elastic displacement velocities, obtained from the measured time-domain seismic wave field data:

$$\mathbf{d}_q^{obs}(s_k) = \int_0^\infty \mathbf{d}_q^{obs}(t)\, e^{-s_k t}\, dt \tag{2}$$

with complex frequency $s_k = \sigma_k + i\omega_k$, where σ_k is the Laplace damping constant and ω_k is the angular frequency with $i = \sqrt{-1}$. Predicted data $\mathbf{d}_q^{sim}(\mathbf{m}, s_k) = \hat{\mathbf{G}}_q \mathbf{v}_q(\mathbf{m}, s_k)$ are defined by the displacement velocity field and depend upon the model parameters $\mathbf{m}$, and an interpolation operator $\hat{\mathbf{G}}_q$ applied to the calculated velocity field in the vicinity of the detector for the source with index q. The velocity components $\mathbf{v}_q^k = \left(v_{q,x}^k, v_{q,y}^k, v_{q,z}^k\right)$ satisfy the system of finite-difference elastic equations for each complex frequency s_k (Virieux 1986):

$$\mathbf{K}(b, \kappa, \mu)_q^k\, \mathbf{v}_q^k = \mathbf{f}_q^k \quad . \tag{3}$$

The explicit expression of the finite-difference operator $\mathbf{K}\left(b,\kappa,\mu\right)_q^k$ can be found in (Petrov, Newman 2012, 2014). We minimize the objective functional in eq. (1) using the nonlinear conjugate gradient method (NLCG) following Polyak and Ribi`ere (1969) and Petrov, Newman (2014) with a pseudo-Hessian matrix as a preconditioner (Choi et al. 2008).

3. RAFT RIVER 3D ELASTIC MODEL

We consider the 3D velocity model designed by Nash and Moore (2012). To reduce both the required memory and computing time, we used a part of the model. The model is rotated so that Narrows Zone aligns along the X-axis with a broadside extension of $1266 \le y \le 3894$ (in meters). The depth extent of the model is $0 \le z \le 2268$ (in meters). The distribution of P-wave velocities in the planes $x = 3588, y = 2556$ and $z = 2028$ m are shown in Figures 2, where synthetic data were generated by the Laplace-Fourier domain finite-difference modeling technique (Petrov and Newman 2012). The number of grid nodes employed in the model and simulation were $211 \times 217 \times 191$ with the grid spacing of 12 m. A free surface boundary condition was imposed on the surface z=0. On the other boundaries, the perfectly match layer (PML) boundary condition is applied, with 5 cells in each direction.

There are 49 z-directed dipole point sources uniformly located from x =2520 m to x = 4680 m, along seven lines that span y =1512 m to y =3672 m at 360 m intervals, in the near surface. A total of 636 receiver locations are equally spaced in the well REG-9 at 80 m intervals from the depth z=80 m up to 1760 m; each detector records the x, y, and z components of the velocity displacement field. Every source uses all available detectors. The projections of survey geometry are presented in Figure 2. The inversion region begins at the depths from $z \ge z_0 = 1400$ m. The initial velocity model is composed from exact formation model, excluding Narrows Zone.

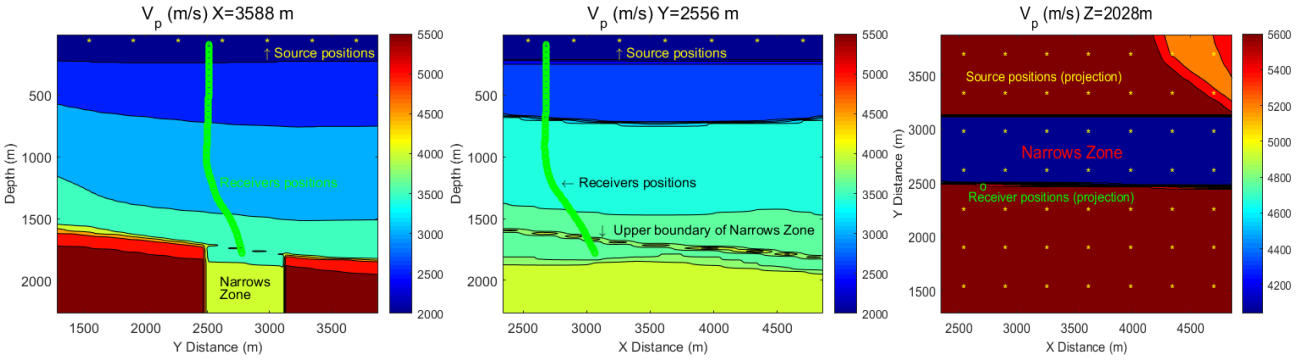

Figure 2: P-wave velocities (m/s) of the Raft River elastic model and seismic survey geometry; surface projection (third panel) is viewed from the North and West.

4. EXPERIMENT DESIGN RESULTS

For the inversion, we used the multistep workflow that involves two loops over frequencies and damping constants. Frequencies were sequentially increased at 5, 7, 12, and 15 Hz with the damping constant decreased at 3,2 and 1 (1/s). The data misfit e_n over the full offset range of 12 km is less than 6%. As Figures 3-4 show, the inversion gives good results around the well, where receivers are placed. This is a region with a size about 1 km for the S wave velocities (Fig. 5b). The P wave velocities are correctly inverted within radius about 1.5--2 km from the well (Fig. 6b). Unfortunately, the geometry of survey and the layered structure of the formation restrict the sensitivity of data and it is not possible to recover distant parts of the Narrows Zone, away from well RG9. Velocity profile inversion results for the Narrows Zone are also shown in Figure 4-6.

5. DISCUSSION

The Raft River elastic model is constructed using geologic features found at the Raft River geothermal field (Ayling and Moore, 2013). It contains two major fault zones that have been identified on the west side of the valley: the bridge fault zone and the horse wells fault zone. The model also contains the Narrows Zone, a shear zone where compression and shear wave velocities are decreased. In this investigation we are interested in the possibility of 3D VSP FWI to image important seismic attributes of the Narrows Zone that can be used to infer fault distributions, and paths of or barriers to fluid flow within the Raft River reservoir. In our inversion studies, thus far, we did not use a smoothed version of the exact model as a starting model, which would include the Narrows fracture zone as in imaging experiments of Lin and Huang (2015). The P-wave velocity results shown in Figures 3 and 6, successfully recovered layered features of the model up to the depth of 2000 m, with deepest sensitivity to the Narrows Zone around the well foot as expected. The S-wave velocity results (Figures 4 and 5) give a sharper image, but are more localized. Within a 600-800m lateral range from the well, S and P velocities images can be directly compared to the well log because of the narrow angle of VSP acquisition. The application of more wide-angle geometry including additional wells would help to overcome under sampling of the wave field, significantly increasing the lateral sensitivity of the VSP measurements beyond several kilometers. Such sensitivity enhancements are expected because of critical and postcritical reflection angles resulting from seismic velocity discontinuities.

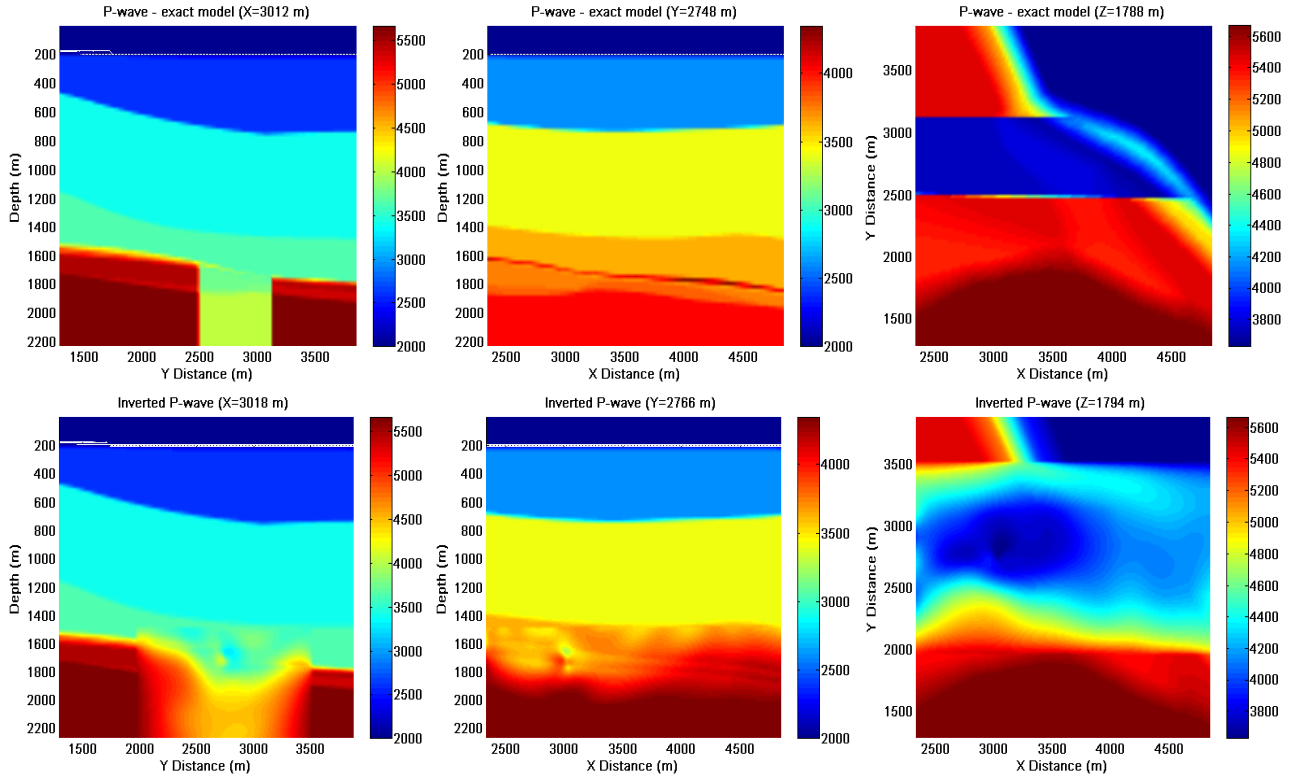

Figure 3: Exact and inverted P-velocities for Narrows Zone.

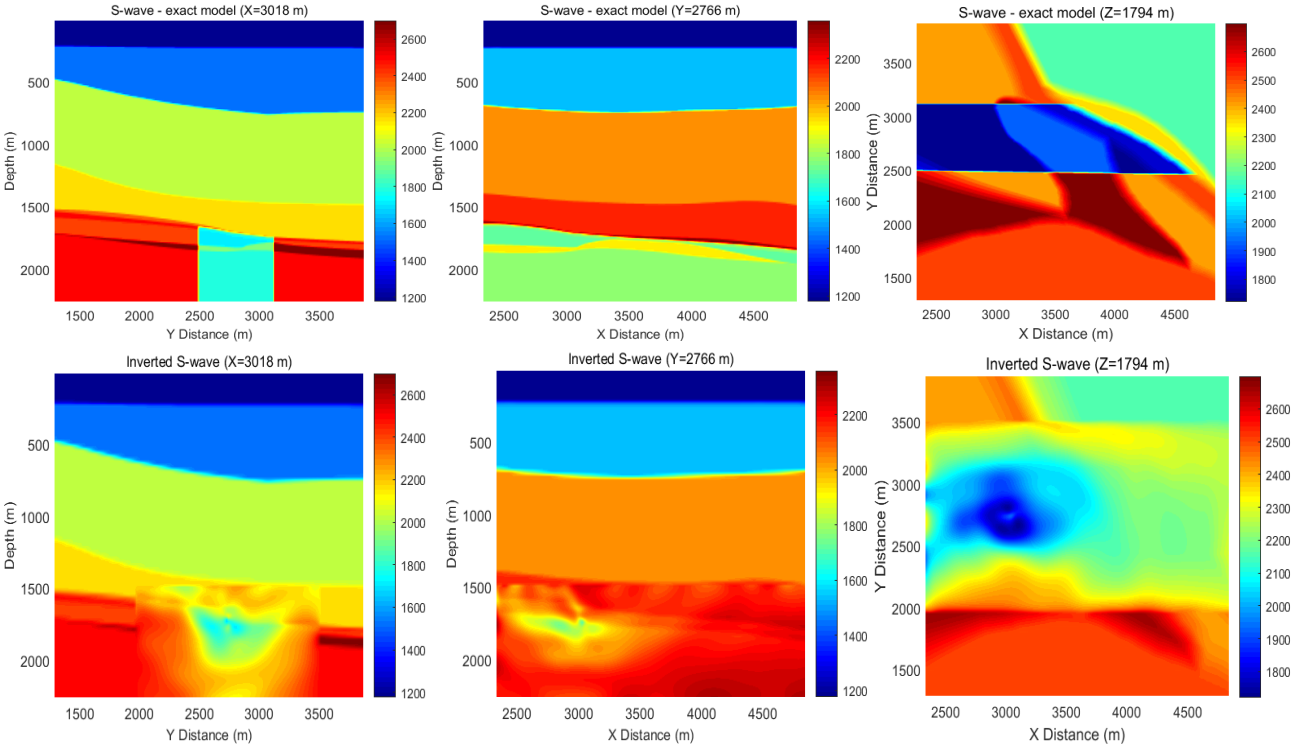

Figure 4: Exact and inverted S-velocities for Narrows Zone.

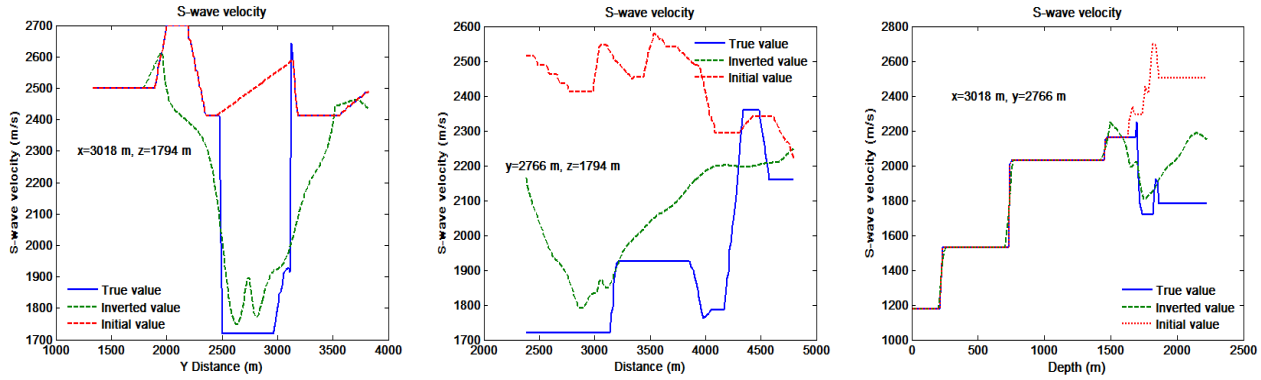

Figure 5: S-wave velocity profiles along the Y- (a), X- (b) and Z-axis (c) for the true, inverted and initial models.

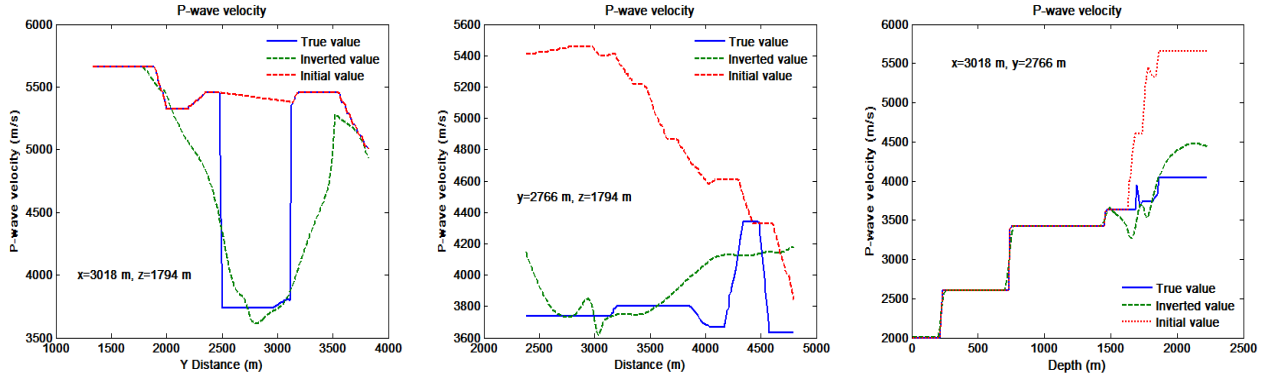

Figure 6: P-wave velocity profiles along the Y- (a), X- (b) and Z-axis (c) for the true, inverted and initial models.

7. CONCLUSIONS

In this paper we reported on our initial survey design experiments for planned VSP data acquisition at Raft River later this year. Our results provide some initial guidance on the VSP survey configuration necessary for imaging seismic attributes within the Narrows Zone. In our design study we employed a 3-D massively parallel elastic waveform inversion algorithm in the Laplace-Fourier domain to update the elastic model. We made no assumptions about dimensionality or geological structure of the Narrows Zone and used a starting model based on the regular formation (interpreted from well logs), which excluded the Narrows Zone. Our findings show the inverted images give the right qualitative structure of the investigated region around the RG9 well; less than 1 km radius from the well, which includes the Narrows Zone. At distances greater than 1 km from the well, the survey geometry is far from optimal and we are not able to produce acceptable reconstructions of the Narrows Zone model. As a result of these findings we continue to experiment with different set of survey design parameters to extend the lateral sensitivity of VSP measurements that meets the targets of the survey within acquisition costs.

8. ACKNOWLEDGEMENTS

This material is based upon work supported by the U.S. Department of Energy Office of Energy Efficiency and Renewable Energy (EERE) Geothermal Technologies Program, under Award Number GT-480010-19823-10. Computational resources were provided by the National Energy Research Scientific Computing (NERSC) Center. All simulations were performed on the NERSC CRAY XE6 and CRAY XC30 supercomputers. The authors acknowledge Joseph Moore, John Queen for providing the 3D elastic Raft River model.

REFERENCES

Ayling B., P. Molling, R. Nye and J. Moore: Fluid geochemistry at the Raft River geothermal field, Idaho: new data and hydrogeological implications, *Proceedings*, 36thWorkshop on Geothermal Reservoir Engineering, SGP-TR-191, (2011).

Ayling, B., and J. Moore: Fluid geochemistry at the Raft River geothermal field, Idaho, USA: New data and hydrogeological implications, *Geothermics*, **47**, (2013), 116-126.

Brossier R., Operto S. *and* Virieux J.: Seismic imaging of complex onshore structures by 2D elastic frequency-domain full-waveform inversion, *Geophysics* **74,** (6), (2009) WCC105–WCC118.

Brossier R., Operto S. and Virieux J: Velocity model building from seismic reflection data by full-waveform inversion, *Geophysical Prospecting*, **63**, (2015) 354–367.

Choi Y., Min D.-J, Shin C.: Frequency-Domain Elastic Full Waveform Inversion Using the New Pseudo-Hessian Matrix: Experience of Elastic Marmousi-2 Synthetic Data, *Bulletin of the Seismological Society of America* **98**, (2008), 2402–2415.

Jones C., J. Moore, W. Teplow and S. Craig: Geology and hydrothermal alteration of the Raft River geothermal system, Idaho, *Proceedings*, 36th Workshop on Geothermal Reservoir Engineering, SGP-TR-191, (2011).

Kapoor, S.,Vigh, D., Wiarda, E. & Alwon, S.: Full waveform inversion around the world: *Proceedings* of the 75th EAGE Conference, Extended Abstracts (2013).

Köhn D., De Nil D., Kurzmann A., Przebindowska A. and Bohlen T.: On the influence of model parametrization in elastic full-waveform tomography, *Geophysical Journal International* **191**, (2012), 325–345.

Lin Y. and Huang L.: Elastic-Waveform Inversion with Compressive Sensing for Sparse Seismic Data: *Proceedings* of the 40th Workshop on Geothermal Reservoir Engineering Stanford University, Stanford, California, January 26-28, SGP-TR-204 (2015).

Mabey, D. R., D. B. Hoover, J. E. O'Donnell, and C. W. Wilson: Reconnaissance geophysical studies of the geothermal systems in southern Raft River valley, Idaho, *Geophysics*, **43**, (1978), 1470-1484.

Nash, G. D., and Moore, J. N.: "Raft River EGS Project: A GIS-Centric Review of Geology": *GRC Transactions*, **36**, (2012), 951 - 958.

Polyak, E., and Ribi`ere, G.: Note sur la convergence desm´ethods conjug´ ees, Rev. Fr. Inr. Rech. Oper., **16**, (1969), 35–43.

Petrov, P. V. and Newman, G. A.: 3D finite-difference modeling of elastic wave propagation in the Laplace-Fourier domain, *Geophysics*, **77**, (2012), T137-T155.

Petrov P.V., Newman G. A.: Three-dimensional inverse modelling of damped elastic wave propagation in the Fourier domain, *Geophysical Journal International* **198**, (2014), 1599–1617.

Plessix R. E., Baeten G., de Maag J. W., Klaasen M., Rujie Z. and Zhifei T.: Application of acoustic full-waveform inversion to a low-frequency large-offset land data set, 80th *Annual International Meeting, SEG, Expanded Abstracts,* (2010) 930–934.

Sirgue L., Barkved O.I., Dellinger J., Etgen J., Albertin U. and Kommedal J.H.: Full waveform inversion: the next leap forward in imaging at Valhall:, *First Break* **28**, (2010) 65–70.

Virieux, J.: P-SV wave propagation in heterogeneous media: Velocity-stress finite-difference method, *Geophysics* **51**, (1986), 889–901.

Williams, P. L., Covington, H. R., and Pierce K. L.: Conozoic Stratigraphy and Tectonic Evolution of the Raft River Basin, Idaho. *In Bill Bonnichsen and R.M. Breckenridge, eds. Conozoic Geology of Idaho: Idaho Bureau* (1982).